Synthesis of Homo- or Hetero-trinuclear Palladium(II)/Platinum(II) Compounds with Bridging Phosphido Ligands. Crystal and Electronic Structures (DFT) of $[N(PPh_3)_2]_2[Pt_3(\mu\text{-}PPh_2)_4(C_6F_5)_4]$ and of Its Oxidation Product $[Pt_3(C_6F_5)_4(\mu\text{-}PPh_2)_4]$†

Ester Alonso,‡ José María Casas,‡ Juan Forniés,*,‡ Consuelo Fortuño,‡ Antonio Martín,§ A. Guy Orpen,§ Constantinos A. Tsipis,*,⊥,|| and Athanassios C. Tsipis||

Departamento de Química Inorgánica and Instituto de Ciencia de Materiales de Aragón, Universidad de Zaragoza-CSIC, 50009 Zaragoza, Spain, School of Chemistry, University of Bristol, Cantock's Close, Bristol, U.K. BS8 1TS, and Laboratory of Applied Quantum Chemistry, Faculty of Chemistry, Aristotle University of Thessaloniki, 54006 Thessaloniki, Greece

Received May 17, 2001

The synthesis of the trinuclear phosphido complexes $[NBu_4]_2[(C_6F_5)_2M(\mu\text{-}PPh_2)_2M'(\mu\text{-}PPh_2)_2M''(C_6F_5)_2]$ (M, M′, M″ = Pd(II), Pt(II), **1**−**5**) is described. A study of the electrochemical behavior of these complexes is reported. The chemical oxidation of the homonuclear platinum derivative involving two electrons yields the complex $[(C_6F_5)_2Pt(\mu\text{-}PPh_2)_2Pt(\mu\text{-}PPh_2)_2Pt(C_6F_5)_2]$ (**6**), which contains Pt in average formal oxidation state 2.67. The structure of the complexes has been established by spectroscopic means, and X-ray diffraction studies have been carried out on **1** and **6**. Quantum chemical calculations at the B3LYP level of theory, using the LANL2DZ basis set, provide a satisfactory description of the structural, bonding, energetic, and electronic properties of these phosphido-bridged trinuclear M_3(II) compounds modeled as $[(CF_3)_2M(\mu\text{-}PH_2)_2M'(\mu\text{-}PH_2)_2M''(CF_3)_2]^{2-}$ (M, M′, M″ = Pd(II), Pt(II), **1M**−**5M**) and the oxidation product $[Pt_3(\mu\text{-}PH_2)_4(CF_3)_4]$ (**6M**).

Introduction

The stability of the M−P bonds in bridging phosphido ligands allows the synthesis of cluster or polynuclear complexes,[1] and their flexibility permits them to adapt to a wide range of distances between the metal centers, which they support. These distances depend on the electronic environment of the metals involved in the polynuclear framework (i.e., their oxidation state and coordination number).

Several years ago we studied the capability of the diphenylphosphido ligand to build up pentafluorophenyl palladium or platinum complexes of different nuclearity,[2] and as a result we described a series of clusters that, essentially based on the typical square planar (more or less distorted) coordination environments of the Pd or Pt centers, adopt the structure required to satisfy the electron demands of the metal centers. To illustrate this, we have collected in Scheme 1 several examples, prepared by us,[3] of the structures adopted indicating the number of skeletal electrons.

Recently, we described the synthesis of the binuclear complex $[(C_6F_5)_2Pt(\mu\text{-}PPh_2)_2Pt(C_6F_5)_2]$ Pt(III)−Pt(III) (Scheme 1b) through oxidation of the $[NBu_4]_2[(C_6F_5)_2Pt(\mu\text{-}PPh_2)_2Pt(C_6F_5)_2]$ Pt(II)−Pt(II) species.[3b] This product is one of the very few complexes known that displays platinum in square planar coordination with a Pt−Pt bond and the Pt−ligand bonds in the same plane. In contrast Pt(III)−Pt(III) complexes displaying octahedral environments with the Pt−Pt bond perpendicular to the equatorial plane have frequently been reported. This fact prompted us to probe further the possibility of using phosphido palladium(II) or platinum(II) complexes to

† Polynuclear Homo- or Heterometallic Palladium(II)/Platinum(II) Pentafluorophenyl Complexes Containing Bridging Diphenylphosphido Ligands. 10. For part 9 see ref 26.

‡ Universidad de Zaragoza-CSIC.

§ University of Bristol.

⊥ To whom correspondence should be addressed for the theoretical calculations.

|| Aristotle University of Thessaloniki.

(1) (a) Baker, R. T.; Fultz, W. C.; Marder, T. B.; Williams, I. D. *Organometallics* **1990**, *9*, 2357, and references therein. (b) Barré, C.; Boudot, P.; Kubicki, M. M.; Moise, C. *Inorg. Chem.* **1995**, *34*, 284. (c) Shyu, S.-G.; Hsu, J.-Y.; Lin, P.-J.; Wu, W.-J.; Peng, S.-M.; Lee, G.-H.; Wen, Y.-S. *Organometallics* **1994**, *13*, 1699. (d) Leoni, P.; Pasquali, M.; Sommovigo, M.; Albinati, A.; Pregosin, P. S.; Ruegger, H. *Organometallics* **1996**, *15*, 2047. (e) Leoni, P.; Pasquali, M.; Fadini, L.; Albinati, A.; Hofmann, P.; Metz, M. *J. Am. Chem. Soc.* **1997**, *119*, 8625. (f) Wachtler, H.; Schuh, W.; Ongania, K.-H.; Wurst, K.; Peringer, P. *Organometallics* **1998**, *17*, 5640. (g) Leoni, P.; Pasquali, M.; Fortunelli, A.; Germano, G.; Albinati, A. *J. Am. Chem. Soc.* **1998**, *120*, 9564. (h) Leoni, P.; Pasquali, M.; Cittadini, V.; Fortunelli, A.; Selmi, M. *Inorg. Chem.* **1999**, *38*, 5257. (i) Bender, R.; Bouaoud, S.-E.; Braunstein, P.; Dusausoy, Y.; Merabet, N.; Raya, J.; Rouag, D. *J. Chem. Soc., Dalton Trans* **1999**, 735. (j) Bender, R.; Braunstein, P.; Dedieu, A.; Ellis, P. D.; Huggins, B.; Harvey, P. H.; Sappa, E.; Tiripicchio, A. *Inorg. Chem.* **1996**, *35*, 1223. (k) Leoni, P.; Manetti, S.; Pasquali, M.; Albinati, A. *Inorg. Chem.* **1996**, *35*, 6045.

(2) Forniés, J.; Fortuño, C.; Navarro, R.; Martínez, F.; Welch, A. J. *J. Organomet. Chem.* **1990**, *394*, 643.

(3) (a) Falvello, L. R.; Forniés, J.; Fortuño, C.; Martínez, F. *Inorg. Chem.* **1994**, *33*, 6242. (b) Alonso, E.; Casas, J. M.; Cotton, F. A.; Feng, X.; Forniés, J.; Fortuño, C.; Tomás, M. *Inorg. Chem.* **1999**, *38*, 5034. (c) Alonso, E.; Forniés, J.; Fortuño, C.; Martín, A.; Orpen A. G. *Organometallics* **2000**, *19*, 2690.

10.1021/om010407s CCC: $20.00
Publication on Web 11/30/2001

Scheme 1

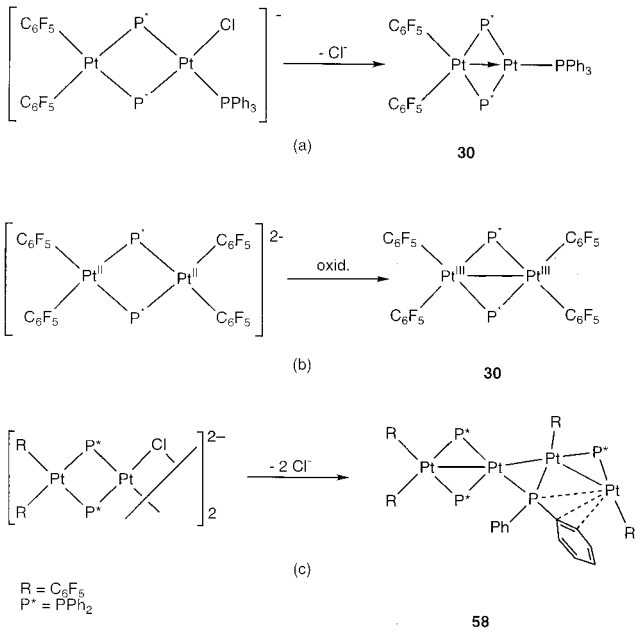

synthesize polynuclear complexes with metal centers in oxidation states higher than II.

In this paper we describe two methods for the syntheses of homo- or hetero-trinuclear complexes $[NBu_4]_2[(C_6F_5)_2M(\mu\text{-}PPh_2)_2M'(\mu\text{-}PPh_2)_2M''(C_6F_5)_2]$ (M, M′, M″ = Pd(II), Pt(II)) with bridging phosphido ligands and study their electrochemical behavior. In addition we describe the synthesis of a novel trinuclear compound $[(C_6F_5)_2Pt(\mu\text{-}PPh_2)_2Pt(\mu\text{-}PPh_2)_2Pt(C_6F_5)_2]$ in which the platinum centers display fractional formal oxidation states of 2.67. Some of the complexes reported are studied by X-ray diffraction methods, and a detailed study of their electronic properties has been carried out by means of density functional theory (DFT).

Results and Discussion

Syntheses of Trinuclear Complexes with All Metal Centers in Oxidation State II. The synthetic strategy for the preparation of these trinuclear compounds was based on previous observations related to pentafluorophenyl phosphido complexes. As has already been noted[2] the tetranuclear compound $[NBu_4]_2[(C_6F_5)_2Pt(\mu\text{-}PPh_2)_2M(\mu\text{-}Cl)_2M(\mu\text{-}PPh_2)_2Pt(C_6F_5)_2]$ (M = Pt, Pd) reacts with bidentate chelating ligands in 1:2 molar ratio to yield binuclear asymmetric complexes $[(C_6F_5)_2Pt(\mu\text{-}PPh_2)_2M(L{-}L)]$. On the other hand, reaction with monodentate ligands in a 1:2 molar ratio results in the formation of yellow binuclear complexes $[NBu_4][(C_6F_5)_2Pt(\mu\text{-}PPh_2)_2MClL]$. The latter, after abstraction of the chloride ligand, yields red (M = Pt) or dark purple (M = Pd) complexes, $[(C_6F_5)_2Pt(\mu\text{-}PPh_2)_2ML]$.[3a] These binuclear 30-electron complexes display a Pt → M dative bond reflected in the short Pt−M distance (2.6571 Å, M = Pd, L = PPh_3) (Scheme 1a). Addition of monodentate L or bidentate L−L ligands results in the formation of 32-electron species, which are yellow and, as expected, do not contain Pt → M dative bonds $[(C_6F_5)_2Pt(\mu\text{-}PPh_2)_2ML_2]$.

Aiming to prepare trinuclear phosphido-containing complexes of palladium or platinum, we decided to use

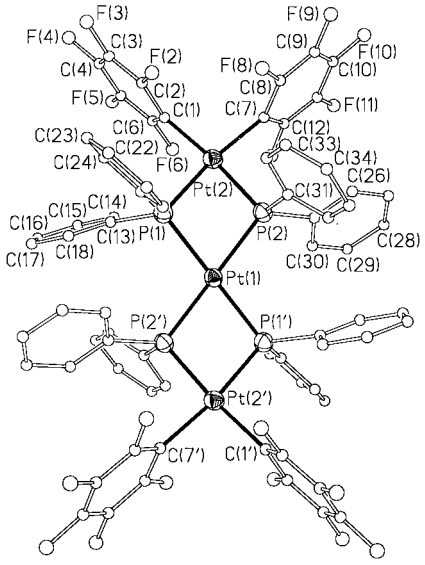

Figure 1. Structure of the complex anion of **1′**, $[Pt_3(\mu\text{-}PPh_2)_4(C_6F_5)_4]^{2-}$.

the *cis*-$[M(C_6F_5)_2(PPh_2)_2]^{2-}$ dianion (prepared in situ by treatment of the neutral compound *cis*-$[M(C_6F_5)_2(PPh_2H)_2]$ (M = Pd, Pt) with n-BuLi)[2] as a chelating diphosphine metalloligand toward the binuclear 30-electron $[(C_6F_5)_2Pt(\mu\text{-}PPh_2)_2MPPh_3]$ (M = Pd, Pt) compounds (Scheme 2). Should these complexes react in a 1:1 molar ratio with displacement of PPh_3, the chelate effect being an important driving force, it would result in a general method for the controlled synthesis of trinuclear phosphido-bridged complexes (see Scheme 2). The isolation of the complexes requires the addition of NBu_4^+ to facilitate crystallization. Complexes **1**, **4**, and **5** were prepared by using this synthetic method (called method *a* below). Attempts to prepare the analogous $[(C_6F_5)_2Pt(\mu\text{-}PPh_2)_2Pt(\mu\text{-}PPh_2)_2Pd(C_6F_5)_2]^{2-}$ compound, by reacting $[(C_6F_5)_2Pt(\mu\text{-}PPh_2)_2PtPPh_3]$ with *cis*-$[Pd(C_6F_5)_2(\mu\text{-}PPh_2)_2]^{2-}$, afforded a mixture of complexes, which we have not been able to separate. Most of the trinuclear complexes, **1**−**4**, have also been prepared by an alternative route involving bridge-assisted substitution processes in which the phosphido metalloligands *cis*-$[M(C_6F_5)_2(PPh_2)_2]^{2-}$, M = Pd or Pt, are treated with *trans*-$[PdCl_2(tht)_2]$ or *cis*-$[PtCl_2(CH_3CN)_2]$ in a 2:1 molar ratio (see Scheme 2, method *b*).

Structural Characterization of Complexes 1−5. Crystal Structure of $[PPN]_2[(C_6F_5)_2Pt(\mu\text{-}PPh_2)_2Pt(\mu\text{-}PPh_2)_2Pt(C_6F_5)_2]\cdot 2Me_2CO$ (1′·2Me$_2$CO). To obtain better crystals, suitable for an X-ray structure determination, complex **1** was also prepared as its PPN^+ salt (see Experimental Section). Thus, a single-crystal X-ray structural determination was carried out on $[PPN]_2[(C_6F_5)_2Pt(\mu\text{-}PPh_2)_2Pt(\mu\text{-}PPh_2)_2Pt(C_6F_5)_2]\cdot 2Me_2CO$ (**1′**·2Me$_2$CO). The structure of the anion of **1′** along with the atom-labeling scheme is shown in Figure 1. Selected bond distances and angles are listed in Table 1. The anion of **1′** is a trinuclear complex containing three Pt(II) atoms with square planar configurations, bridged by diphenylphosphido ligands, while pentafluorophenyl groups act as terminal ligands. In the crystal structure there is an inversion center located at Pt(1); hence both "halves" of the complex are identical. The coordination environments of the Pt(1) and Pt(2) atoms exhibit an

Scheme 2

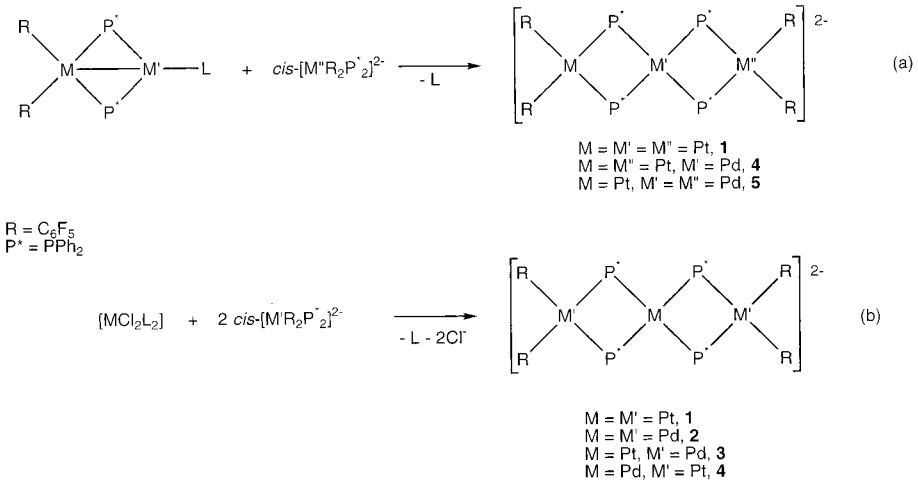

Table 1. Selected Bond Lengths (Å) and Angles (deg) for Complex $[PPN]_2[Pt_3(\mu\text{-}PPh_2)_4(C_6F_5)_4]\cdot 2Me_2CO$ (1′·2Me$_2$CO)[a]

Pt(1)−P(1)	2.364(1)	Pt(1)−P(2)	2.371(1)	Pt(2)−C(7)	2.077(5)
Pt(2)−C(1)	2.085(5)	Pt(2)−P(2)	2.313(1)	Pt(2)−P(1)	2.324(1)

P(1)−Pt(1)−P(2′)	105.08(5)	P(1)−Pt(1)−P(2)	74.92(5)
C(7)−Pt(2)−C(1)	91.0(2)	C(7)−Pt(2)−P(2)	94.17(14)
C(1)−Pt(2)−P(2)	174.53(13)	C(7)−Pt(2)−P(1)	170.66(14)
C(1)−Pt(2)−P(1)	98.10(13)	P(2)−Pt(2)−P(1)	76.79(5)
C(19)−P(1)−Pt(2)	108.0(2)	C(13)−P(1)−Pt(2)	116.1(2)
C(19)−P(1)−Pt(1)	114.9(2)	C(13)−P(1)−Pt(1)	115.4(2)
Pt(2)−P(1)−Pt(1)	100.04(5)	C(31)−P(2)−Pt(2)	112.4(2)
C(25)−P(2)−Pt(2)	111.9(2)	C(31)−P(2)−Pt(1)	113.7(2)
C(25)−P(2)−Pt(1)	117.0(2)	Pt(2)−P(2)−Pt(1)	100.14(5)

[a] The symmetry transformation used to generate equivalent P(2′) atom is $-x, -y, -z$.

essentially planar geometry, with the angle between the two planes being equal to 152.7°. The Pt···Pt distance of 3.592(1) Å strongly suggests that no intermetallic bond is present. As a consequence, the Pt−P−Pt bond angles are quite large (ca. 100°), and the inner P−Pt−P angles small (ca. 75°), as previously observed in analogous phosphido-bridged platinum complexes without Pt−Pt bonds. The Pt−P and Pt−C distances are in the range commonly found for complexes of this kind.[3−8]

The IR spectra of **1**, **2**, and **4** show two absorptions of similar intensity (in the range 760−780 cm^{-1}, see Experimental Section) assignable to the X-sensitive mode of the C_6F_5 groups,[4] in accord with the presence of two mutually *cis* C_6F_5 groups per metal center. In the IR spectrum of complex **3** these bands are not well resolved, whereas in complex **5**, which contains two C_6F_5 groups bonded to a Pt center and two C_6F_5 groups bonded to Pd, three absorptions, one of them with higher intensity, were observed in this region.

The ^{19}F NMR spectra of **1**−**4** (see Experimental Section) show three signals with intensities in the ratio 2:2:1. One of them, with platinum satellites for complexes **1** and **4**, is characteristic of the *o*-F atoms, and the two other signals at higher field are due to *m*-F and *p*-F atoms. This ^{19}F NMR pattern indicates that all C_6F_5 moieties are equivalent in solution. The two halves of each pentafluorophenyl group are likewise equivalent. The ^{19}F NMR spectrum of **5** shows six signals in 2:2:2:2:1:1 intensity ratio: two signals in the *o*-F region, one of them with platinum satellites, two signals due to the two types of *m*-F, and two signals (intensity ratio 1:1) due to the two types of *p*-F atom. This pattern reflects the presence of two equivalent C_6F_5 groups bonded to a platinum center and two equivalent C_6F_5 groups bonded to palladium, as well as the magnetic equivalence of the two halves of all C_6F_5 moieties in solution.

The ^{31}P NMR spectra of **1**−**5** show signals in the high-field region (δ P from −105.3 to −126.4 ppm). The spectrum of **1** shows a singlet signal in accord with the presence of four equivalent P atoms for the isotopomer in which ^{195}Pt atoms are not present (29.3% abundance). This signal is flanked by platinum satellites, due to the presence of five isotopomers in which one, two, or three metal centers are ^{195}Pt. The signals due to the five isotopomers are strongly overlapped; hence only the doublet due to the isotopomer in which the central platinum atom is ^{195}Pt (A_4X spin system, 14.9% abundance) can be unambiguously identified from the spectrum and the $^1J_{Pt,P}$ value of 1606 Hz can be extracted. In complex **2**, in which all the metal atoms are palladium, the four P atoms are equivalent, and therefore only one singlet signal is observed in the ^{31}P NMR spectrum. The spectrum of complex **3** shows the central singlet and the expected doublet due to the ^{195}Pt (A_4X spin system, 33.7% abundance), $^1J_{Pt,P} = 1485$ Hz. The spectrum of complex **4** shows the central singlet due to the isotopomer in which ^{195}Pt atoms are not present (all P atoms are equivalent, 43.9% abundance) and platinum satellites due to the isotopomers with one ($AA'A''A'''X$ spin system, 44.7% abundance) or two ^{195}Pt atoms ($AA'A''A'''XX'$ spin system, 11.3% abundance). From the signals due to the isotopomer with one ^{195}Pt the $^1J_{Pt,P}$ and N ($J_{A,A''} + J_{A,A'''}$) values can be extracted and are found to be 1502 and 129 Hz, respectively. In complex **5**, which contains two types of P atom (two P atoms bridging two palladium centers and two P atoms bridging one palladium and one platinum center), the spec-

(4) Usón, R.; Forniés, J. *J. Adv. Organomet. Chem.* **1988**, *28*, 188.
(5) Alonso, E.; Forniés, J.; Fortuño, C.; Martín, A.; Rosair, G. M.; Welch, A. J. *Inorg. Chem.* **1997**, *36*, 4426.
(6) Falvello, L. R.; Forniés, J.; Fortuño, C.; Martín, A.; Martínez-Sariñena, A. P. *Organometallics* **1997**, *16*, 5849.
(7) Alonso, E.; Forniés. J.; Fortuño, C.; Tomás, M. *J. Chem. Soc., Dalton Trans.* **1995**, 3777.
(8) (a) Mercer, W. C.; Geoffroy, G. L.; Rheingold, A. L. *Organometallics* **1985**, *4*, 1418. (b) Carty, A. J. *Adv. Chem. Ser.* **1982**, *196*, 163. (c) Mercer, W. C.; Whittle, R. R.; Burkhardt, E. W.; Geoffroy, G. L. *Organometallics* **1985**, *4*, 68.

trum shows a pattern typical of an AA′XX′ spin system, the X part exhibiting platinum satellites. All data, which can be extracted from the spectrum, are collected in the Experimental Section. The δP values in phosphido derivatives are very informative about structure. Usually these values are found in the range of +300 to +50 ppm for complexes in which the metals bridged by PR_2 groups are joined by a metal−metal bond and in the range of +50 to −200 ppm when the metals are not bonded.[8] In our experience, the δP values in complexes with large M−M distances (no metal−metal bond) appear at lower fields in the "M(μ-PPh_2)M" and "M(μ-PPh_2)(μ-X)M" fragments (δP = 48.9 ppm in $[Pd_4(\mu\text{-}PPh_2)_2(\mu\text{-}Cl)_4(C_6F_5)_4]^{2-}$;[5] −6.9 ppm in $[Pt_4(\mu\text{-}PPh_2)_4(C_6F_5)_4(CO)_2]$;[6] 1.4 (X = Cl) or −31.4 (X = OH) ppm in $[Pt_3(\mu\text{-}PPh_2)_3(\mu\text{-}X)(C_6F_5)_2(PPh_3)_2]$[7]) than in the "M($\mu$-$PPh_2$)$_2$M" fragments ($\delta$P = −121.1 and −109.7 ppm in $[Pt_2(\mu\text{-}PPh_2)_2(C_6F_5)_2(C_5H_5N)(CO)]$;[3a] −132.0 ppm in $[Pt_2(\mu\text{-}PPh_2)_2(C_6F_5)_2(phen)]$[2]). So, the δP values in complexes **1**−**5** are found in the range expected for complexes in which two PPh_2 groups bridge two metal centers without a metal−metal bond. In addition, it is noteworthy that δP in the homotrinuclear palladium complex **2**, −106.4 ppm, appears at lower field than in the homotrinuclear platinum complex **1**, −126.4 ppm. Similarly, the δP value for PPh_2 groups bonded to two palladium centers in the heterotrinuclear complex **5**, −105.3 ppm, is higher than for the two PPh_2 groups bonded to one palladium and one platinum center in the same derivative **5**, −123.6 ppm. The same trend can be observed in the symmetric heterotrinuclear complexes **3** (Pd_2Pt) and **4** (Pt_2Pd): −110.3 and −118.0 ppm, respectively. Likewise, the dinuclear complexes $[(C_6F_5)_2M(\mu\text{-}PPh_2)_2M'(C_6F_5)_2]^{2-}$ (−105.6, −128.2, and −146.9 ppm for Pd_2, PdPt, and Pt_2 derivatives, respectively)[2] and the tetranuclear derivatives $[\{(C_6F_5)_2Pt(\mu\text{-}PPh_2)_2M(\mu\text{-}Cl)\}_2]^{2-}$ (−113.1 or −133.2 ppm for M = Pd or Pt, respectively)[2] show the same relationship. These data lead us to conclude that in a diphenyphosphido complex the P atom of the PPh_2 group is shielded upon substitution of a palladium by a platinum center.

Oxidation Reactions. The complexes **1**−**5** were studied by cyclic voltammetry. In all cases the experiments were carried out in CH_2Cl_2 solutions using $[NBu_4][PF_6]$ as the supporting electrolyte, a Pt disk electrode, and a calomel reference electrode (SCE). The very low solubility of the complexes makes it necessary to work with dilute solutions, ca. 1×10^{-5} M. All complexes show oxidation waves in the range between −0.3 and 0.1 V The cyclic voltammograms for complexes **1** and **4** exhibit quasi-reversible oxidation processes in which the anodic and cathodic peaks appear at −10 and −217 mV (**1**) and −160 and −278 mV (**4**) at 100 mV s^{-1} scan rate, but the separation between them varies with scan rate (see Figure 2). However, in the same potential range, complexes **2**, **3**, and **5** show only the oxidation waves at −170, −86, and −182 mV, respectively, the reduction peak not being perceptible. In addition, the electrochemical behavior of complexes **2**−**5** also involves an irreversible oxidation at higher potentials, 886, 984, 1.076, and 714 mV, respectively, at 100 mV s^{-1}.

Chemical oxidation of complexes **1**−**5** was attempted with Ag^+. Reaction of a yellow suspension of $[NBu_4]_2[(C_6F_5)_2Pt(\mu\text{-}PPh_2)_2Pt(\mu\text{-}PPh_2)_2Pt(C_6F_5)_2]$, **1**, with $AgClO_4$ (1:2 molar ratio) in CH_2Cl_2 solutions for 3 h resulted in the precipitation of metallic silver and the formation of a dark red solution. After workup of the mixture the neutral trinuclear cluster $[(C_6F_5)_2Pt(\mu\text{-}PPh_2)_2Pt(\mu\text{-}PPh_2)_2Pt(C_6F_5)_2]$, **6**, was obtained as a deep red solid, which contains two metal centers in formal oxidation state III and one in formal oxidation state II and hence contains a $[Pt_3]^{8+}$ core. No evidence for the formation of the trinuclear $[(C_6F_5)_2Pt(\mu\text{-}PPh_2)_2Pt(\mu\text{-}PPh_2)_2Pt(C_6F_5)_2]^+$ cation with all the Pt centers in formal oxidation state III, $[Pt_3]^{9+}$, was obtained. The trinuclear mixed-valence compound **6** can be chemically reduced to the Pt(II) derivative **1** by reaction with NBu_4BH_4 in CH_2Cl_2 in a 1:2 molar ratio.

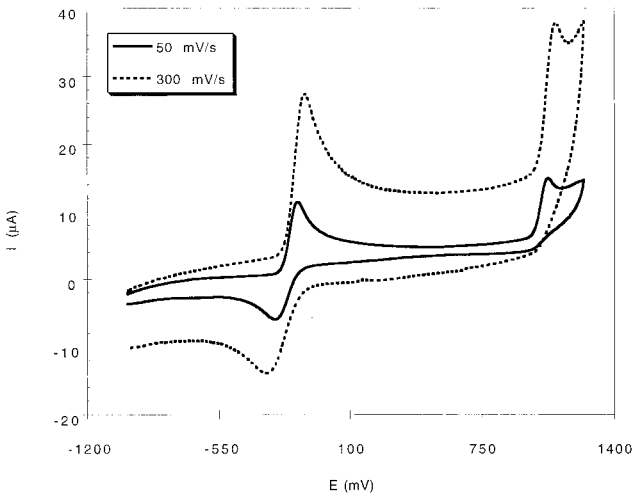

Figure 2. Cyclic voltammogram for complex **4** in the range −1.00 to 1.25 V at 50 mV s^{-1} (solid line) scan rate showing the quasi-reversible oxidation processes at $E_a = -160$ mV, $E_c = -270$ mV and an irreversible oxidation at 1.076 mV. Dotted line CV at 300 mV s^{-1} scan rate ($E_a = -119.7$ mV, $E_c = -308.3$ mV and an irreversible oxidation at 1115 mV.

Attempts to oxidize the other trinuclear complexes (**2**−**5**) with Ag^+ under similar conditions afforded very dark solutions from which a mixture of Pt/Pd-containing complexes was obtained. We have not been able to separate and identify the compounds in these mixtures, although the ^{31}P NMR spectra of the mixtures seem to indicate that no complexes analogous to **6** are present. These mixtures are currently being investigated further.

Crystal Structure of $[(C_6F_5)_2Pt(\mu\text{-}PPh_2)_2Pt(\mu\text{-}PPh_2)_2Pt(C_6F_5)_2]\cdot n\text{-}C_5H_{12}$ ($6\cdot n\text{-}C_5H_{12}$). The structure of complex **6** along with the atom-labeling scheme is shown in Figure 3. Selected bond distances and angles are listed in Table 2. It is a neutral trinuclear compound involving three Pt atoms [formally Pt(III)−Pt(III)···Pt(II)] bridged by diphenylphosphido ligands, while the pentafluorophenyl groups act as terminal ligands. In the crystal structure of **6** there is a 2-fold axis passing through all three platinum atoms. The Pt···Pt intermetallic distances are quite different; the Pt(1)···Pt(2) distance of 2.776(1) Å is indicative of a Pt(1)−Pt(2) bond, whereas the Pt(2)···Pt(3) distance is 3.674(1) Å, ruling out any Pt−Pt bond. The framework of the "Pt(2)(μ-PPh_2)$_2$Pt(3)$(C_6F_5)_2$" moiety is quite similar to that described for complex **1′**. However, some structural parameters of the "$(C_6F_5)_2$Pt(1)(μ-PPh_2)$_2$Pt(2)" moiety are quite different. As a result of the Pt(1)−Pt(2) bond, the inner Pt−P−Pt bond angles are smaller in **6**,

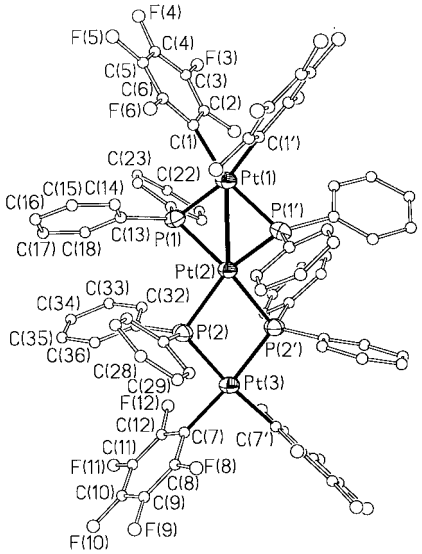

Figure 3. Structure of complex $[Pt_3(C_6F_5)_4(\mu\text{-}PPh_2)_4]$ (**6**).

Table 2. Selected Bond Lengths (Å) and Angles (deg) for Complex $[Pt_3(C_6F_5)_4(\mu\text{-}PPh_2)_4]\cdot n\text{-}C_5H_{12}$ ($6\cdot n\text{-}C_5H_{12}$)[a]

Pt(1)−Pt(2)	2.777(1)	Pt(1)−C(1)	2.078(10)	Pt(1)−P(1)	2.280(3)
Pt(2)−P(1)	2.299(3)	Pt(2)−P(2)	2.380(2)	Pt(3)−C(7)	2.054(10)
Pt(3)−P(2)	2.274(3)				
C(1′)−Pt(1)−C(1)	86.7(6)	C(1)−Pt(1)−P(1′)	163.7(3)		
C(1)−Pt(1)−P(1)	85.2(3)	P(1′)−Pt(1)−P(1)	105.97(12)		
C(1)−Pt(1)−Pt(2)	136.6(3)	P(1′)−Pt(2)−P(1)	104.70(13)		
P(1′)−Pt(2)−P(2)	149.41(9)	P(1)−Pt(2)−P(2)	96.69(9)		
P(2)−Pt(2)−P(2′)	73.74(12)	P(2)−Pt(2)−Pt(1)	143.13(6)		
C(7′)−Pt(3)−C(7)	89.0(5)	C(7)−Pt(3)−P(2′)	174.3(3)		
C(7)−Pt(3)−P(2)	96.6(3)	P(2′)−Pt(3)−P(2)	77.77(13)		
Pt(1)−P(1)−Pt(2)	74.66(8)	Pt(3)−P(2)−Pt(2)	104.25(10)		

[a] The symmetry transformation used to generate equivalent primed atoms is $-x + 2, y, -z + 3/2$.

74.66(8)°, while the P−Pt−P angles are larger, at around 105°. This complex is another excellent example of the well-recognized flexibility of bridging phosphido ligands which are able to adapt the M−P−M bond angle to the M−M distance, according to the existence or not of an intermetallic bond. The coordination environments of Pt(1) and Pt(3) are planar, but that of Pt(2) is quite distorted, probably due to the difference of the two inner P−Pt(2)−P angles (104.70(13)° and 73.74(12)°). Thus the dihedral angle formed by the Pt(2)−P(1)−P(1a) and Pt(2)−P(2)−P(2a) planes is 38.4°. The Pt−P and Pt−C distances are in the range commonly found for this kind of complex.

The ^{19}F NMR spectrum of **6** (in deuteroacetone, HDA, as well as in CD_2Cl_2) at room temperature shows three signals in a 2:2:1 intensity ratio: one of them, with platinum satellites, in the usual region for *o*-F atoms and two signals at higher fields due to *m*-F and *p*-F atoms. This pattern indicates that in solution the four C_6F_5 groups are equivalent, as are the two halves of each pentafluorophenyl group. This is not in accord with the structure of **6** in the solid state. Nevertheless, in agreement with the solid-state structure, the spectrum at 218 K in CD_2Cl_2 shows six signals (intensity ratio 2:2:1:2:1:2): two signals, with platinum satellites, due to two types of *o*-F, two signals due to two types of *m*-F, and two signals for two types of *p*-F atoms. This pattern is in accord with the presence of two types of C_6F_5 groups: two C_6F_5 groups bonded to a Pt(III) center and two C_6F_5 groups bonded to a Pt(II) one. The chemical shifts indicate that at room temperature none of the C_6F_5 groups are bonded to a paramagnetic Pt center. A variable-temperature study of the dynamic process gives a ΔG value of 43 kJ·mol^{-1}.

The ^{31}P NMR spectrum of **6** in CD_2Cl_2 at 218 K is in accord with the structure in the solid state. It shows two well-separated signals, as expected for an AA′XX′ spin system for the four P atoms, at 262.3 and −124.2 ppm. The downfield signal indicates the presence of two diphenylphosphido groups bridging two metal centers joined by metal−metal bond. Both signals appear as broad pseudotriplets, and all we can extract from them is the value of 112 Hz for N ($J_{AX} + J_{AX'}$). Both signals are flanked by platinum satellites due to the three isotopomers, in which one platinum center is ^{195}Pt (14.8% each one) and the two $^1J_{Pt,P}$ values can be extracted for each signal. Signals due to the three isotopomers in which two platinum centers are ^{195}Pt (7.5% abundance each one) as well as to the one in which the three metal atoms are ^{195}Pt (3.8% abundance) were not observed. No signals have been observed in the ^{31}P spectra of **6** at room temperature either in CD_2Cl_2 or in HDA. Nevertheless at 323 K in HDA a very broad signal centered at ca. 60 ppm just emerges from the baseline. The NMR spectra of **6** indicate that at room temperature a dynamic process, which renders the two terminal Pt centers magnetically equivalent, operates in solution. These data are consistent with this being the higher barrier process noted above.

This kind of dynamic behavior constitutes a clear example of M−M bond migration which takes place through an intramolecular electron transfer and which is favored by the flexibility of the phosphido ligand. Dynamic metal−metal bonds is not an unknown phenomenon and it is being studied with great interest.[9]

The characteristic absorption bands of the pentafluorophenyl groups in the IR spectrum near 950 cm^{-1} are very informative.[4] In this region of the spectrum, complex **6** shows two absorptions of similar intensities at 963 and 955 cm^{-1}, whereas the starting material, the anionic platinum(II) species **1**, shows only one absorption at 950 cm^{-1} The shift of the frequency of one of the absorptions to higher wavenumbers by 15 cm^{-1} is in agreement with an increase in the formal oxidation state in one of the two metal centers bonded to C_6F_5 groups. Complex **6**, which involves two different *cis*-Pt-$(C_6F_5)_2$ moieties, shows three absorptions assignable to the X-sensitive mode of the C_6F_5 groups.

Computational Studies Using Density Functional Theory

(a) Qualitative Description of the Electronic Structures of the Complexes $[Pt_3(\mu\text{-}PPh_2)_4(C_6F_5)_4]^{n-}$ (n = 2, 0). An understanding of the Pt−Pt interactions and their influence on the reactivity and physical properties of $[Pt_3(\mu\text{-}PPh_2)_4(C_6F_5)_4]^{n-}$ (n = 2, 0) and related compounds is based on the electronic structure

(9) (a) Bailey, D. A.; Balch, A. L.; Fossett, L. A.; Olmstead, M. M.; Reedy, E. *Inorg. Chem.* **1987**, *26*, 2413. (b) Chisholm, M. H.; Clark, D. L.; Hampden-Smith, M. J. *J. Am. Chem. Soc.* **1989**, *111*, 574. (c) Houser, E. J.; Rauchfuss, T. B.; Wilson, S. R. *Inorg. Chem.* **1993**, *32*, 4069. (d) Houser, E. J.; Venturelli, A.; Rauchfuss, T. B.; Wilson, S. R. *Inorg. Chem.* **1995**, *34*, 6402. (e) Liu, X.-Y.; Riera, V.; Ruiz, M. A.; Tiripicchio, A.; Tiripicchio-Camellini, M. *Organometallics* **1996**, *15*, 983.

Scheme 3

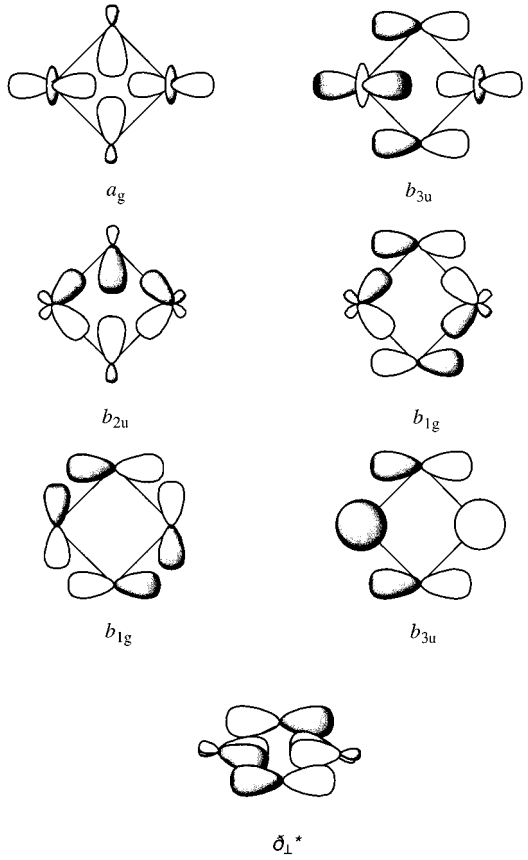

and bonding in their bridge $Pt_2(\mu\text{-}PR_2)_2$ regions. Generally, allocation of the Pt−Pt-based valence electrons into molecular orbitals of σ, π, δ, δ*, π*, and σ* symmetries (in the framework of the through-ring bonding theory in edge-sharing dimers of square planar complexes suggested by Alvarez et al.[10]) could provide a wealth of information regarding the chemistry that these trinuclear platinum systems will possess.

Qualitatively, one expects four bridge MOs, which arise from the interaction of the lone-pair combination of the bridging PR_2 unit with the Pt_2L_4 orbitals of the same symmetry. These MOs having a_g, b_{3u}, b_{2u}, and b_{1g} symmetry (first four orbitals shown in Scheme 3), along with three more orbitals exhibiting high electron density on the bridge atoms and having b_{1g}, b_{3u}, and π* symmetry are depicted schematically in Scheme 3. The π* MO, together with σ*, has distinctly lower d character than the other six orbitals, and its presence allows d^7-d^7 molecules to exist.[11] The d^8-d^8 $[L_2Pt(II)(\mu\text{-}PR_2)_2Pt(II)L_2]^{2-}$ compounds will have two bridging bonds and then a sufficient number of electrons to fill up all six σ, σ*, π, π*, δ, and δ* PtPt orbitals resulting in no intermetallic Pt−Pt bond. In contrast, the d^7-d^7 $[L_2Pt(III)(\mu\text{-}PR_2)_2Pt(III)L_2]$ compounds will have only 10 electrons to occupy the six PtPt orbitals, two bridging bonds resulting in a formal single Pt−Pt bond. These MO architectures built up from the simple extended Hückel calculations[11] are quantitatively supported by DFT calculations at the B3LYP level of theory as some

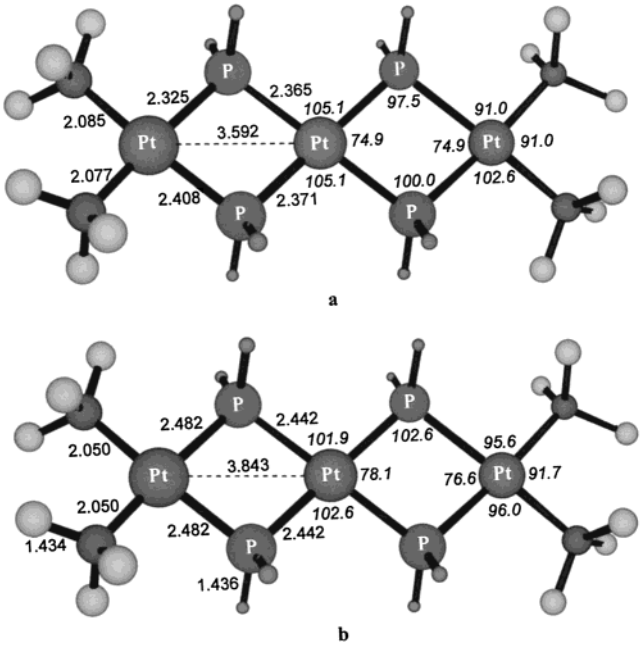

Figure 4. Structural parameters of $[Pt_3(\mu\text{-}PH_2)_4(CF_3)_4]^{2-}$ (**1M**) model compound taken from the crystal structure of $[Pt_3(\mu\text{-}PPh_2)_4(C_6F_5)_4]^{2-}$ (a) and those of a fully optimized geometry at the B3LYP/LANL2DZ level of theory exhibiting D_{2h} symmetry (b) (bond lengths in Å, bond angles in deg).

of us have previously reported[3b] in a detailed DFT and structural study of d^8-d^8 $[L_2Pt(II)(\mu\text{-}PH_2)_2Pt(II)L_2]^{2-}$ and d^7-d^7 $[L_2Pt(III)(\mu\text{-}PH_2)_2Pt(III)L_2]$ (L = C_6F_5) complexes. In the latter study the ability of such DFT methods (B3LYP functional, LANL2DZ, 6-31G basis set) to reproduce experimental geometry and identify the Pt···Pt bonding interactions and its variation on oxidation in this class of complex was demonstrated.

(b) Electronic Properties and Bonding of the Trinuclear $[Pt_3(\mu\text{-}PH_2)_4(CF_3)_4]^{2-}$ (1M) Compound. The structural parameters of the model compound $[Pt_3(\mu\text{-}PH_2)_4(CF_3)_4]^{2-}$ (**1M**) shown in Figure 4a are those of the real $[Pt_3(\mu\text{-}PPh_2)_4(C_6F_5)_4]^{2-}$ dianion (**1**) determined experimentally by X-ray crystallography. Selected geometrical parameters of the fully optimized geometry at the B3LYP/LANL2DZ level of theory of the model compound **1M** are shown in Figure 4b. The optimized geometry corresponds to a planar structure exhibiting D_{2h} symmetry. The two structures differ mainly in the deviation of the coordination geometry of the real $[Pt_3(\mu\text{-}PPh_2)_4(C_6F_5)_4]^{2-}$ dianion (**1**) from planarity (the square planar geometries of one terminal and the central platinum atoms form an angle of 27.3°). Such a deviation from planarity of **1** results in a structure for **1M**, which is about 152 kcal·mol^{-1} higher in energy than the optimized planar D_{2h} structure. The stabilization of the nonplanar geometry of **1** adopting a chair conformation could be attributed to both the bulk and electronic effects of the bridging PPh_2 and the terminal C_6F_5 ligands. In effect, the substitution of PPh_2 and C_6F_5 ligands by the simpler PH_2 and CF_3 ligands, respectively, to obtain a computationally convenient size, affects the computed geometrical parameters of **1M**. In general terms, the computed Pt−P bond lengths of both the terminal and central Pt(II) atoms in the optimized planar D_{2h} structure are longer by 0.074 Å (0.127 Å)

(10) Aullón, G.; Alemany, P.; Alvarez, S. *J. Organomet. Chem.* **1994**, *478*, 75.
(11) Shaik, S.; Hoffmann, R.; Fisel, C. R.; Summerville, R. H. *J. Am. Chem. Soc.* **1980**, *102*, 4555.

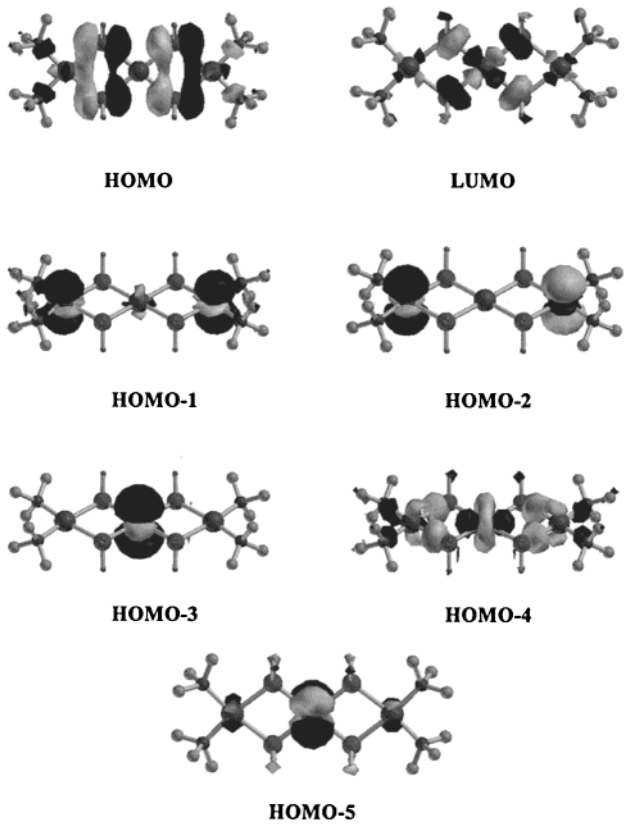

Figure 5. Highest occupied (HOMO) and lowest unoccupied (LUMO) molecular orbitals of $[Pt_3(\mu\text{-}PH_2)_4(CF_3)_4]^{2-}$ (**1M**), along with a few more frontier MOs exhibiting predominantly d_{z^2} character localized either on the central or terminal Pt(II) atoms.

and 0.071 Å (0.077 Å), respectively, as compared to those of **1M** corresponding to the experimentally determined geometry. The same is also true for the Pt···Pt distance in **1M** being 0.251 Å longer than the experimentally estimated value (3.843 vs 3.592 Å). In contrast, the computed bond angles are in fairly good agreement with the experimental values, differing at most by 6.6°. The computed dipole moments of both structures are 0.0 D.

The HOMO−LUMO energy gap of **1M** is 4.65 eV (4.62 eV for D_{2h} structure), illustrating a well-defined closed-shell electronic configuration consistent with the diamagnetic nature of the real compound. Moreover, a group of five frontier MOs with eigenvalues in the region of −1.52 to −2.14 eV exhibiting predominantly Pt d character (Figure 5) is expected along with the HOMO at −1.18 eV to be involved in the two-electron oxidation of $[Pt_3(\mu\text{-}PH_2)_4(CF_3)_4]^{2-}$ (**1M**) to $[Pt_3(\mu\text{-}PH_2)_4(CF_3)_4]$ (**6M**). In effect the two electrons involved in the oxidation process are electrons occupying the MOs localized mainly on the P and Pt(II) atoms. In addition, upon removing the two electrons occupying the MOs, there are appropriate d orbital residues located on the oxidized metal centers to favor two-center−two-electron interactions leading to the formation of a Pt(III)−Pt(III) intermetallic bond. Notice that the HOMO exhibiting a_g symmetry is a nonbonding MO being primarily an out-of-phase combination of p_x wave functions of the P atoms. On the other hand the LUMO with a_u symmetry corresponds to Pt−P antibonding interactions mainly localized on the central PtP_4 chromophore.

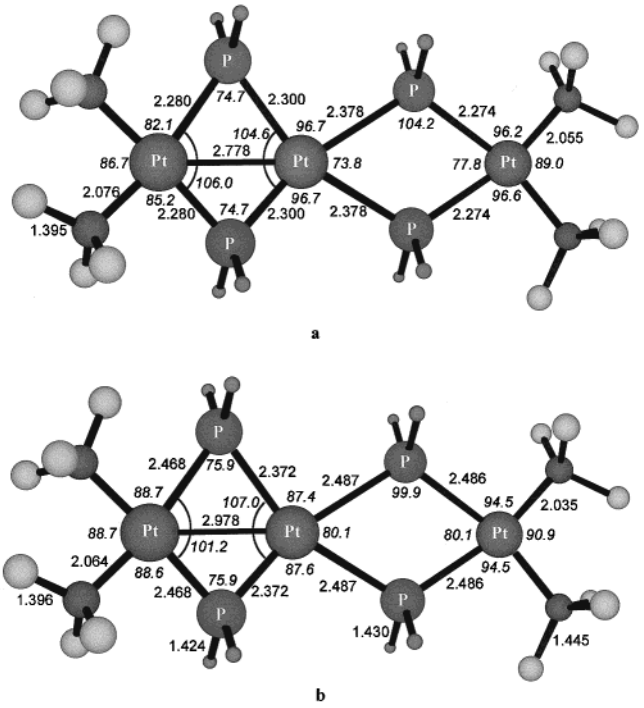

Figure 6. Structural parameters of $[Pt_3(\mu\text{-}PH_2)_4(CF_3)_4]$ (**6M**) taken from the crystal structure of $[Pt_3(\mu\text{-}PPh_2)_4(C_6F_5)_4]$ (a) and those of a fully optimized geometry at the B3LYP/LANL2DZ level of theory (b) (bond lengths in Å, bond angles in deg).

(c) Electronic Properties and Bonding of the Trinuclear $[Pt_3(\mu\text{-}PH_2)_4(CF_3)_4]$ (6M) Compound. Exploring the existence of intermetallic Pt(III)−Pt(III) interactions in the oxidized product inferred from the relatively short Pt(III)−Pt(III) distance of 2.776 Å in the real $[Pt_3(\mu\text{-}PPh_2)_4(C_6F_5)_4]$ compound **6**, two possible structures of the model $[Pt_3(\mu\text{-}PH_2)_4(CF_3)_4]$ compound have been studied at the B3LYP level of theory. The first corresponds to the experimentally determined geometry of $[Pt_3(\mu\text{-}PPh_2)_4(C_6F_5)_4]$ **6** shown in Figure 6a (**6M**). The second structure corresponds to the B3LYP/LANL2DZ fully optimized geometry of **6M** with the selected structural parameters shown in Figure 6b. In both structures the coordination environments of Pt(1) and Pt(3) are planar, but that of Pt(2) is quite distorted. The computed dihedral angle formed by the Pt(2)−P(1)−P(1a) and Pt(2)−P(2)−P(2a) planes is 15.0°, much lower than the experimentally determined value of 38.4° for **6**. The fully optimized structure of **6M** was found at about 181 kcal·mol^{-1} lower in energy than the structure with the experimentally determined geometrical parameters. The substitution of PPh_2 and C_6F_5 by PH_2 and CF_3 ligands, respectively, affects the computed geometrical parameters of **6M**. The Pt−P bond lengths of both the terminal and central Pt atoms are overestimated at the fully optimized structure. Thus, the terminal Pt(III)−P and Pt(II)−P bond lengths are longer by 0.19 and 0.21 Å, respectively, while the central Pt(III)−P bond lengths are longer by 0.07 Å (0.11 Å) as compared to those of **6M** with the experimentally determined structural parameters. The same is also true for the Pt(III)−Pt(III) and Pt(III)···Pt(II) distances in **6M**, being 0.202 and 0.134 Å longer than the experimentally estimated values (2.978 vs 2.776 Å and 3.808 vs 3.674 Å). The computed bond angles are in fairly good

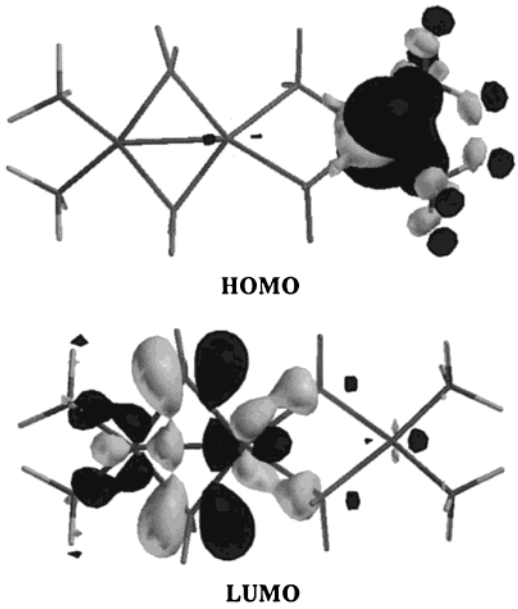

Figure 7. HOMO and LUMO of $[Pt_3(\mu\text{-}PH_2)_4(CF_3)_4]$ (**6M**).

agreement with the experimental values, differing at most by 9.3°. In contrast to the unoxidized Pt(II) (d^8) complex the computed structure of **6** illustrates that the central Pt(III) (d^7) prefers to adopt a nonplanar four-coordinated geometry, in line with the experimental observations. The computed dipole moment of **6M** is 6.7 D (7.90 D for **6M** with the experimentally determined geometry).

The HOMO of **6M**, with an eigenvalue of −6.93 eV (−7.45 eV for the optimized structure), corresponds to Pt(II)−CF_3 bonding interactions depicted schematically in Figure 7. The Pt(II) orbitals participating in these bonding interactions are mainly an in-phase combination of d_{z^2} and d_{yz} orbitals. Further oxidation of **6** would be expected to occur on the terminal Pt(II) atom, affording a fully oxidized Pt_3(III) compound. However, such an oxidation would occur at high oxidation potential (approximately higher than 6.93 V according to Koopmans' theorem). This is consistent with the observation that chemical oxidation to the $[Pt_3]^{9+}$ cation was not detected in any of the oxidation processes. The LUMO (Figure 7), with an eigenvalue of −5.21 eV (−5.82 eV), corresponds to σ^* Pt(III)−Pt(III) antibonding interactions involving significant contributions from the bridging phosphido ligands. The LUMO′ character is consistent with **6** being reversibly reduced to **1**. The HOMO−LUMO energy gap is 1.72 eV (1.63 eV), indicating that **6** has a singlet diamagnetic ground state. Calculations performed on the triplet state, at the same level of theory, illustrated that the latter is 40 kcal·mol^{-1} higher in energy.

Looking for bonding molecular orbitals which are likely to contribute to Pt(III)−Pt(III) intermetallic interactions, the most important, with an eigenvalue of −11.82 eV (−11.40 eV), is depicted schematically in Figure 8. This MO was found at much lower energies than those of all other metal-based orbitals and exhibits strong Pt(III)−Pt(III) σ-bonding character.

From the analysis of Mulliken population results given in Figure 9 the following conclusions can be drawn: (a) The terminal Pt atoms acquire positive net atomic charges, while the central one is negatively charged with a computed negative net atomic charge of

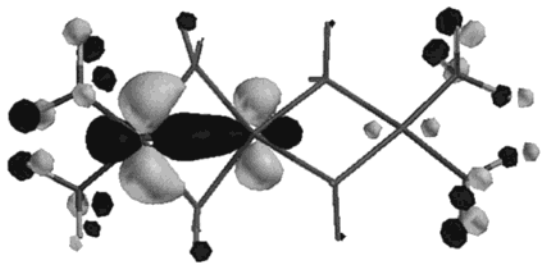

Figure 8. The σ-bonding molecular orbital of $[Pt_3(\mu\text{-}PH_2)_4(CF_3)_4]$ (**6M**) contributing to Pt(III)−Pt(III) intermetallic interactions.

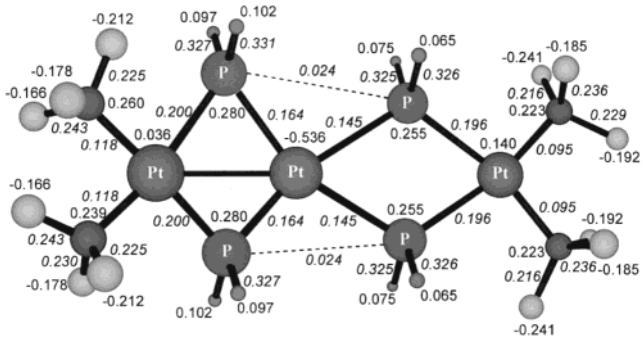

Figure 9. Net atomic charges and bond overlap populations of $[Pt_3(\mu\text{-}PH_2)_4(CF_3)_4]$ (**6M**) obtained from a Mulliken population analysis.

−0.536 charge units, being equal to that of the central platinum atom of the unoxidized compound **1M**. In the latter compound the terminal Pt atoms are almost neutral, with net atomic charges of only −0.003 charge units. Obviously, the central Pt atom is predicted to be the nucleophilic center of the $[Pt_3(\mu\text{-}PH_2)_4(CF_3)_4]$ compound (**6M**). (b) The bond overlap populations of the Pt−P bonds indicate that the formation of the Pt−Pt intermetallic bond strengthens the Pt−P bonds (bop values of 0.164 and 0.200 in the four-member ring involving Pt−Pt interactions as compared to those of 0.145 and 0.196 in the four-member ring without Pt−Pt interactions). Surprisingly, the bop values do not correlate with the Pt−P bond lengths, as it should be expected for covalent bonding and suggesting that in the solid state other factors, such as packing forces and steric interactions, are operating.[12] Most importantly, the oxidation results in a significant weakening of the Pt−P bonds formed by the bridging phosphido ligands (compare the bop of the Pt−P bonds of the central and terminal Pt atoms of the precursor dianion, being 0.201 and 0.265, respectively, to those of its oxidized product). Upon oxidation of **1M** to **6M**, there is a remarkable increase of the positive net atomic charge on the P atoms of the bridging phosphido ligands (0.18 in **1M** and 0.26 and 0.28 in **6M**). (c) Interestingly, weak P···P interactions exist between the phosphido ligands bridging the central and terminal Pt atoms, reflected in the P···P bond overlap population of 0.024.

(d) Electronic Properties and Bonding of Trinuclear $[Pd_3(\mu\text{-}PH_2)_4(CF_3)_4]^{2-}$ (2M), $[(CF_3)_2Pd(\mu\text{-}PH_2)_2Pt(\mu\text{-}PH_2)_2Pd(CF_3)_2]^{2-}$ (3M), $[(CF^3)_2Pt(\mu\text{-}PH_2)_2Pd(\mu\text{-}PH_2)_2Pt(CF_3)_2]^{2-}$ (4M), and $[(CF^3)_2Pt(\mu\text{-}PH_2)_2Pd(\mu\text{-}PH_2)_2Pd(CF_3)_2]^{2-}$ (5M) Compounds. Our last models were the other trinuclear compounds involving the

(12) Martín, A.; Orpen, A. G. *J. Am. Chem. Soc.* **1996**, *118*, 1464.

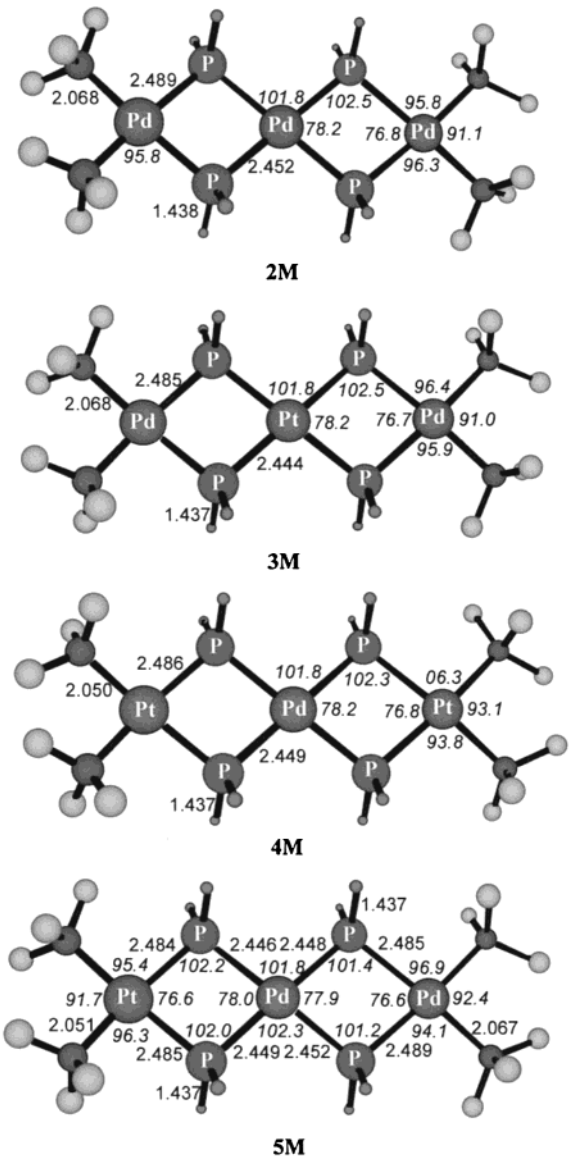

Figure 10. B3LYP/LANL2DZ fully optimized structures of trinuclear $[Pd_3(\mu\text{-}PH_2)_4(CF_3)_4]^{2-}$ (**2M**), $[(CF_3)_2Pd(\mu\text{-}PH_2)_2Pt(\mu\text{-}PH_2)_2Pd(CF_3)_2]^{2-}$ (**3M**), $[(CF_3)_2Pt(\mu\text{-}PH_2)_2Pd(\mu\text{-}PH_2)_2Pt(CF_3)_2]^{2-}$ (**4M**), and $[(CF_3)_2Pt(\mu\text{-}PH_2)_2Pd(\mu\text{-}PH_2)_2Pd(CF_3)_2]^{2-}$ (**5M**) compounds (bond lengths in Å, bond angles in deg).

Pd(II)···Pd(II)···Pd(II), **2M**, Pd(II)···Pt(II)···Pd(II), **3M**, Pt(II)···Pd(II)···Pt(II), **4M**, and Pt(II)···Pd(II)···Pd(II), **5M**, skeletons. The structural parameters of the B3LYP/LANL2DZ fully optimized geometries of **2M**−**5M** are shown in Figure 10. Surprisingly, there are no significant structural changes upon substitution of Pd by Pt atoms. The Pd−P and Pt−P bonds have almost the same length. The same is also true for the P−Pd−P and P−Pt−P bond angles. The only significant change observed is the lengthening of the Pd−C bond by 0.018 Å with respect to the Pt−C one.

The HOMOs at −0.858, −0.982, −1.056, and −0.97 eV for **2M**, **3M**, **4M**, and **5M**, respectively, correspond to nonbonding MOs, being primarily an out-of-phase combination of p_x wave functions of the P atoms. A representative HOMO along with a LUMO for **2M** is depicted schematically in Figure 11. The HOMO's character indicates that a two-electron oxidation of the

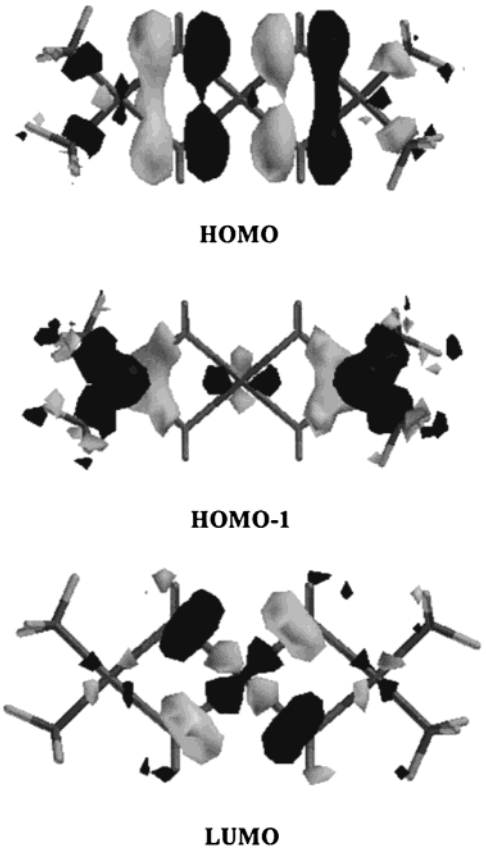

Figure 11. HOMO, HOMO-1, and LUMO of $[Pd_3(\mu\text{-}PH_2)_4(CF_3)_4]^{2-}$ (**2M**).

complexes would be expected to occur primarily on the bridging phosphido ligands instead of the metal atoms. However, the HOMO-1 shown also in Figure 11 corresponding to M−P and M−C bonding interactions localized on the terminal metal atoms having also a small contribution from the $d_{x^2-y^2}$ orbital of the central metal atom could support the oxidation of the metal atoms, as well.

Based upon the well-established maximum hardness principle (MHP) the stability of the trinuclear dianions follow the trend **1M** > **3M** > **4M** > **5M** > **2M** with η = 2.309, 2.119, 1.929, 1.888, and 1.823 eV, respectively, the hardness η defined by Parr and Pearson[13] as $\eta = 1/2(IP - EA) = 1/2(\epsilon_{LUMO} - \epsilon_{HOMO})$ and where IP and EA are the first vertical ionization potential and electron affinity of the species, which in the framework of Koopman's theorem can be approximated by ϵ_{HOMO} and ϵ_{LUMO} with opposite sign, respectively. In general terms it can be seen that the stability of the compounds increases as the number of Pt atoms increases.

Concluding Remarks

This paper presents general methods for the synthesis of homo- or hetero-trinuclear phosphido-bridged complexes. Cyclic voltammetry studies reveal the possibility of oxidation of all of them. However, only the homonuclear platinum derivative **1** is chemically oxidized to a compound, which can be fully characterized, compound **6**. This species contains platinum in formal

(13) (a) Parr R. G.; Pearson R. G. *J. Am. Chem. Soc.*, **1983**, *105*, 7512. (b) Pearson R. G. *J. Chem. Educ.* **1987**, *64*, 561. (c) Pearson R. G. *Acc. Chem. Res.* **1992**, *26*, 250.

oxidation state 2.67, i.e., two platinum centers in oxidation state III and the other one in II. This compound is noteworthy since (a) as far as we know, it is only the second example of an homonuclear triplatinum species with an average oxidation state above II. The first, $[Pt_3(Hnonp)_2(NO_3)(bipy)_3](ClO_4)_2(NO_3)$, has been described recently.[14] (b) In complex **6** the Pt−Pt bond is not perpendicular (or nearly perpendicular) to the platinum coordination planes and the platinum coordination planes are not parallel (or nearly parallel), as is the case in $[Pt_3(Hnonp)_2(NO_3)(bipy)_3](ClO_4)_2(NO_3)$ and in most polynuclear platinum complexes exhibiting oxidation states higher than II.[15] (c) The Pt−Pt bond is clearly localized, in the solid state, between two platinum centers, displaying very different distances between the metal centers. However, this complex is rather flexible in solution, and at room temperature all the platinum environments are identical on the NMR time scale, indicating an intramolecular M−M bond migration. The use of DFT computational techniques provides a satisfactory description of the structural, bonding, energetic, and electronic properties of the trinuclear M_3(II) complexes $[(CF_3)_2M(\mu\text{-}PH_2)_2M'(\mu\text{-}PH_2)_2M''(CF_3)_2]^{2-}$ (M, M′, M″ = Pd(II), Pt(II), models for **1**−**5**) and the oxidation product $[Pt_3(\mu\text{-}PH_2)_4(CF_3)_4]$ (a model for **6**).

Experimental Section

General Procedures and Materials. C, H, and N analyses, IR, NMR, and mass spectra, and cyclic voltammetry were performed as described elsewhere.[3b] Cyclic voltammetric studies were performed under argon using an EG&G model 273 potentiostat in conjunction with a three-electrode cell. The three-electrode system consists of a platinum disk working electrode, a platinum wire auxiliary electrode, and a saturated calomel reference electrode (SCE) separated from the test compartment by a fine-porosity frit. We used diluted solutions in the test compounds because of the low solubility of the trinuclear complexes in CH_2Cl_2 and 0.1 M in $[NBu_4][PF_6]$ as supporting electrolyte. The measurements for complexes **1**−**5** were carried out in ca. 1×10^{-4} M CH_2Cl_2 solutions. Literature methods were used to prepare *cis*-$[M(C_6F_5)_2(PPh_2H)_2]$,[2] $[(C_6F_5)_2Pt(\mu\text{-}PPh_2)_2M(PPh_3)]$,[3a] $[PdCl_2(tht)_2]$,[16] and $[PtCl_2(CH_3CN)_2]$.[17]

Safety Note: Perchlorate salts of metal complexes with organic ligands are potentially explosive. Only small amounts of material should be prepared, and these should be handled with great caution.

Synthesis of $[NBu_4]_2[(C_6F_5)_2Pt(\mu\text{-}PPh_2)_2Pt(\mu\text{-}PPh_2)_2Pt(C_6F_5)_2]$ (1). (a) To a THF solution (10 mL) of *cis*-$[Pt(C_6F_5)_2(PPh_2H)_2]$ (0.069 g, 0.077 mmol) was added at −78 °C LiBu (hexane solution, 0.16 mmol). After 15 min stirring, $[(C_6F_5)_2Pt(\mu\text{-}PPh_2)_2Pt(PPh_3)]$ (0.105 g, 0.077 mmol) was added. The mixture, after reaching room temperature, was stirred for 1 h. The resulting solution was evaporated to dryness, and the residue was treated with ^{i}PrOH (15 mL). After filtration of a small solid residue, a yellow solution was obtained. The addition of NBu_4ClO_4 (0.114 g, 0.333 mmol) results in the precipitation of a yellow solid, which was filtered off and washed with 2 × 2 mL of ^{i}PrOH. The yellow solid was recrystallized from acetone/chloroform, yielding **1** (0.095 g, 50% yield).

(b) To a THF solution (10 mL) of *cis*-$[Pt(C_6F_5)_2(PPh_2H)_2]$ (0.300 g, 0.333 mmol) was added at −78 °C LiBu (hexane solution, 0.68 mmol). After 15 min stirring, $[PtCl_2(CH_3CN)_2]$ (0.058 g, 0.166 mmol) was added and the resulting mixture was stirred, after reaching room temperature, for 13 h. After evaporation to dryness, the residue was treated with ^{i}PrOH (15 mL), yielding a yellow solution. The addition of NBu_4ClO_4 (0.114 g, 0.333 mmol) results in the precipitation of a yellow solid, which was filtered off, washed with 3 × 2 mL of ^{i}PrOH, and recrystallized from acetone/chloroform (0.288 g, 70% yield). Anal. Found (calcd for $C_{104}F_{20}H_{112}N_2P_4Pt_3$): C 50.2 (50.4); H 4.6 (4.5); N 1.2 (1.1). IR (Nujol, X-sensitive C_6F_5): 768 and 777 cm^{-1}. Λ_M = 180 Ω^{-1} cm^2 mol^{-1}. ^{19}F NMR (293 K, deuteroacetone, 282.4 MHz): δ −112.5 (8 *o*-F, $^3J_{Pt,F}$ = 281.3 Hz), −167.0 (8 *m*-F), −168.6 (4 *p*-F) ppm. ^{31}P NMR (293 K, deuteroacetone, 121.4 MHz): δ −126.4 ($^1J_{Pt(1),P}$ = 1606 Hz) ppm. For X-ray purposes $[PPN]_2[(C_6F_5)_2Pt(\mu\text{-}PPh_2)_2Pt(\mu\text{-}PPh_2)_2Pt(C_6F_5)_2]$, **1′**, has been obtained (0.723 g, 85% yield) similarly to **1** by using *cis*-$[PtCl_2(CH_3CN)_2]$ (0.097 g, 0.277 mmol), *cis*-$Li_2[Pt(C_6F_5)_2(PPh_2)_2]$ (0.555 mmol), and $PPNCl\cdot 1/2CH_2Cl_2$ (0.345 g, 0.555 mmol). Anal. Found (calcd for $C_{144}F_{20}H_{100}N_2P_8Pt_3$): C 56.2 (56.3); H 3.2 (3.3); N 0.9 (0.9).

Synthesis of $[NBu_4]_2[(C_6F_5)_2Pd(\mu\text{-}PPh_2)_2Pd(\mu\text{-}PPh_2)_2Pd(C_6F_5)_2]$ (2). Complex **2** was prepared similarly to **1**, method b, by using *cis*-$[Pd(C_6F_5)_2(PPh_2H)_2]$ (0.200 g, 0.246 mmol), LiBu (hexane solution, 0.50 mmol), and $[PdCl_2(tht)_2]$ (0.044 g, 0.123 mmol) and 12 h stirring. The addition of NBu_4ClO_4 (0.084 g, 0.245 mmol) results in the precipitation of an orange solid, which was filtered off, washed with 3 × 2 mL of ^{i}PrOH, and recrystallized from acetone/chloroform (**2**, 0.147 g, 54% yield). Anal. Found (calcd for $C_{104}F_{20}H_{112}N_2P_4Pd_3$): C 56.1 (56.4); H 4.9 (5.1); N 1.3 (1.3). IR (Nujol, X-sensitive C_6F_5): 761 and 769 cm^{-1}. Λ_M = 187 Ω^{-1} cm^2 mol^{-1}. ^{19}F NMR (293 K, deuteroacetone, 282.4 MHz): δ −109.5 (8 *o*-F), −165.9 (8 *m*-F), −167.4 (4 *p*-F) ppm. ^{31}P NMR (293 K, deuteroacetone, 121.4 MHz): δ −106.4 ppm.

Synthesis of $[NBu_4]_2[(C_6F_5)_2Pd(\mu\text{-}PPh_2)_2Pt(\mu\text{-}PPh_2)_2Pd(C_6F_5)_2]$ (3). Complex **3** was prepared similarly to **1**, method b, by using *cis*-$[Pd(C_6F_5)_2(PPh_2H)_2]$ (0.200 g, 0.246 mmol), LiBu (hexane solution, 0.50 mmol), and $[PtCl_2(CH_3CN)_2]$ (0.043 g, 0.123 mmol) and 6 h stirring. The addition of NBu_4ClO_4 (0.084 g, 0.245 mmol) results in the precipitation of a solid, which was filtered off and washed with 3 × 2 mL of ^{i}PrOH. The recrystallization from acetone/chloroform gives **3** as a yellow solid (0.209 g, 74% yield). Anal. Found (calcd for $C_{104}F_{20}H_{112}N_2P_4Pd_2Pt$): C 54.1 (54.3); H 4.6 (4.9); N 1.1 (1.2). IR (Nujol, X-sensitive C_6F_5): 775 cm^{-1}, broad. Λ_M = 149 Ω^{-1} cm^2 mol^{-1}. ^{19}F NMR (293 K, deuteroacetone, 282.4 MHz): δ −109.5 (8 *o*-F), −165.9 (8 *m*-F), −167.4 (4 *p*-F) ppm. ^{31}P NMR (293 K, deuteroacetone, 121.4 MHz): δ −110.3 ($^1J_{Pt,P}$ = 1485 Hz) ppm.

Synthesis of $[NBu_4]_2[(C_6F_5)_2Pt(\mu\text{-}PPh_2)_2Pd(\mu\text{-}PPh_2)_2Pt(C_6F_5)_2]$ (4). Complex **4** was prepared similarly to **1**, method a, by using *cis*-$[Pt(C_6F_5)_2(PPh_2H)_2]$ (0.075 g, 0.083 mmol), LiBu (hexane solution, 0.17 mmol), $[(C_6F_5)_2Pt(\mu\text{-}PPh_2)_2Pd(PPh_3)]$ (0.105 g, 0.083 mmol), and NBu_4ClO_4 (0.057 g, 0.166 mmol). Complex **4** was obtained as an orange solid (0.142 g, 72%).

Complex **4** was prepared similarly to **1**, method b, by using *cis*-$[Pt(C_6F_5)_2(PPh_2H)_2]$ (0.200 g, 0.222 mmol), LiBu (hexane solution, 0.45 mmol), and $[PdCl_2(tht)_2]$ (0.039 g, 0.111 mmol) and 2 h stirring. The addition of NBu_4ClO_4 (0.076 g, 0.222 mmol) results in the precipitation of a solid, which was filtered off and washed with 3 × 2 mL of ^{i}PrOH. The recrystallization from acetone/chloroform gives complex **4** as an orange solid (0.201 g, 76% yield). Anal. Found (calcd for $C_{104}F_{20}H_{112}N_2P_4PdPt_2$): C 51.8 (52.2); H 4.3 (4.7); N 1.1 (1.2). IR (Nujol, X-sensitive C_6F_5): 768 and 777 cm^{-1}. Λ_M = 175 Ω^{-1} cm^2 mol^{-1}. ^{19}F NMR (293 K, deuteroacetone, 282.4 MHz): δ −114.0 (8 *o*-F, $^3J_{Pt,F}$ = 323.4 Hz), −168.5 (8 *m*-F), −170.2 (4 *p*-F) ppm. ^{31}P NMR (293 K, deuteroacetone, 121.4 MHz): δ −118.0 ($^1J_{Pt(1),P}$ = 1502 Hz, N = 129 Hz) ppm.

(14) Oskui, B.; Sheldrick, W. S. *Eur. J. Inorg. Chem.* **1999**, 1325.
(15) Cotton, F. A.; Walton, R. A. *Multiple Bonds between Metal Atoms*, 2nd ed.; Oxford University Press: Oxford, U.K., 1992.
(16) Usón, R.; Forniés, J.; Martinez, F.; Tomás, M. *J. Chem. Soc., Dalton Trans.* **1980**, 888.
(17) Hofmann, K. A.; Bugge, G. *Chem. Ber.* **1907**, *40*, 1772.

Table 3. Crystal Data and Structure Refinement for $[PPN]_2[Pt_3(\mu\text{-}PPh_2)_4(C_6F_5)_4]\cdot 2Me_2CO$ (1′·2Me$_2$CO) and $[Pt_3(C_6F_5)_4(\mu\text{-}PPh_2)_4]\cdot n\text{-}C_5H_{12}$ (6·*n*-C$_5$H$_{12}$)

	1′·2Me$_2$CO	6·*n*-C$_5$H$_{12}$
empirical formula	$C_{144}H_{102}F_{20}N_2P_8Pt_3\cdot 2Me_2CO$	$C_{72}H_{40}F_{20}P_4Pt_3\cdot n\text{-}C_5H_{12}$
fw	3189.46	2066.34
temp (K)	293(1)	293(1)
wavelength (Å)	0.71073	0.71073
cryst syst	triclinic	monoclinic
space group	$P\bar{1}$	$C2/c$
unit cell dimens		
a (Å)	12.663(2)	19.368(6)
b (Å)	15.332(3)	24.760(7)
c (Å)	19.264(5)	19.525(5)
α (deg)	67.20(2)	90
β (deg)	85.37(2)	117.90(2)
γ (deg)	75.34(1)	90
volume (Å^3)	3335.0(12)	8275(4)
Z	1	4
density(calc) (Mg/m^3)	1.588	1.659
abs coeff (mm^{-1})	3.317	5.220
F(000)	1578	3952
diffractometer	Siemens P3m	Siemens P3m
2θ range for data collect. (deg)	3.3−50 ($+h, \pm k, \pm l$)	3.3−50 ($+h, +k, \pm l$)
refinement method	full-matrix least-squares on F^2	
goodness-of-fit on F^2 [b]	1.204	1.027
final R indices ($I > 2\sigma(I)$)[a]	R1 = 0.0359, wR2 = 0.0843	R1 = 0.0447, wR2 = 0.0972
R indices (all data)	R1 = 0.0487, wR2 = 0.0903	R1 = 0.0824, wR2 = 0.1220

[a] $R1 = (\sum||F_o| - |F_c||)/\sum|F_o|$; $wR2 = [\sum w(F_o^2 - F_c^2)^2/\sum w(F_c^2)^2]^{1/2}$. [b] Goodness-of-fit $= [\sum w(F_o^2 - F_c^2)^2/(n_{obs} - n_{param})]^{1/2}$. $w = [\sigma^2(F_o) + (g_1P)^2 + g_2P]^{-1}$; $P = [\max(F_o^2; 0) + 2F_c^2]/3$.

Synthesis of $[NBu_4]_2[(C_6F_5)_2Pt(\mu\text{-}PPh_2)_2Pd(\mu\text{-}PPh_2)_2Pd(C_6F_5)_2]$ (5). Complex **5** was prepared similarly to **1**, method a, by using *cis*-$[Pd(C_6F_5)_2(PPh_2H)_2]$ (0.072 g, 0.088 mmol), LiBu (hexane solution, 0.18 mmol), $[(C_6F_5)_2Pt(\mu\text{-}PPh_2)_2Pd(PPh_3)]$ (0.111 g, 0.088 mmol), and NBu_4ClO_4 (0.058 g, 0.168 mmol). Complex **5** was obtained as an orange solid (0.091 g, 45%). Anal. Found (calcd for $C_{104}F_{20}H_{112}N_2P_4Pd_2Pt$): C 54.2 (54.3); H 4.7 (4.9); N 1.2 (1.2). IR (Nujol, X-sensitive C_6F_5): 759, 770, and 780 cm^{-1}. Λ_M = 201 Ω^{-1} cm^2 mol^{-1}. ^{19}F NMR (293 K, deuteroacetone, 282.4 MHz): δ −110.9 (4 *o*-F), −114.5 (4 *o*-F, $^3J_{Pt,F}$ = 319.6 Hz), −167.5 (4 *m*-F), −168.5 (4 *m*-F), −169.0 (2 *p*-F), −170.1 (2 *p*-F) ppm. ^{31}P NMR (293 K, deuteroacetone, 121.4 MHz): δ −105.3 (P_A), −123.6 (P_X, $^1J_{Pt,P}$ = 1639 Hz) ppm; $J_{A,X}$ = 316 Hz, $J_{A,X'}$ = 36 Hz, $|J_{A,A'}|$ (or $|J_{X,X'}|$) = 206 Hz, $|J_{X,X'}|$ (or $|J_{A,A'}|$) = 146 Hz.

Preparation of $[(C_6F_5)_2Pt(\mu\text{-}PPh_2)_2Pt(\mu\text{-}PPh_2)_2Pt(C_6F_5)_2]$ (6). To a yellow suspension of **1** (0.150 g, 0.060 mmol) in CH_2Cl_2 (30 mL) was added $AgClO_4$ (0.035 g, 0.169 mmol), and the mixture was stirred, at room temperature and in the dark, for 3 h. The resulting red solution was filtered through Celite to eliminate the Ag^0 and passed through silica gel (1 cm^2 × 10 cm). The filtrate was evaporated to 1 mL and kept in a freezer (−20 °C) for 4 h. The resulting red crystals (**6**) were filtered off and washed with 2 × 0.5 mL of $CHCl_3$ (0.080 g, 67% yield). Anal. Found (calcd for $C_{72}F_{20}H_{40}P_4Pt_3$): C 43.0 (43.4); H 2.0 (2.0). IR (Nujol): 963 and 955 cm^{-1}; 796, 787, and 776 cm^{-1}. FAB$^+$ MS: *m*/*z* 1994 ($C_{72}F_{20}H_{40}P_4Pt_3$) ^{19}F NMR (293 K, CD_2Cl_2, 282.4 MHz): δ −118.5 (8 *o*-F, $^3J_{Pt,F}$ = 298.0 Hz), −164.3 (8 *m*-F), −161.6 (4 *p*-F) ppm. ^{19}F NMR (218 K, CD_2Cl_2, 282.4 MHz): δ −118.3 (4 *o*-F, $^3J_{Pt,F}$ = 282.4 Hz), −120.1 (4 *o*-F, $^3J_{Pt,F}$ = 273.9 Hz), −158.4 (2 *p*-F), −162.8 (4 *m*-F), −163.7 (2 *p*-F), −165.0 (4 *m*-F) ppm. ^{31}P NMR (218 K, CD_2Cl_2, 121.4 MHz): δ 262.3 ($^1J_{Pt,P}$ = 1208 and 1261 Hz, $N = J_{AX} + J_{AX'}$ = 112 Hz), −124.2 ($^1J_{Pt,P}$ = 1894 and 1542 Hz) ppm.

Reaction of 6 with NBu_4BH_4. To a red solution of **6** (0.100 g, 0.050 mmol) in CH_2Cl_2 (20 mL) was added NBu_4BH_4 (0.030 g, 0.116 mmol), and the mixture was stirred for 30 min. After filtering through Celite, the solution was evaporated to dryness, and $CHCl_3$ (3 mL) was added. The mixture was kept in a freezer (−20 °C) for 5 h, and the yellow solid **1** was filtered off and washed with 2 × 1 mL of cold $CHCl_3$ (0.074 g, 60% yield).

X-ray Structure Determinations. Crystals of 1′·2Me$_2$CO suitable for X-ray diffraction studies were obtained by slow diffusion of *n*-hexane into a solution of 0.020 g of **1′** in 4 mL of Me_2CO. Crystals of **6**·*n*-C$_5$H$_{12}$ suitable for X-ray diffraction studies were obtained by slow diffusion of *n*-pentane into a solution of 0.015 g of **6** in 5 mL of CH_2Cl_2. In both cases, diffracted intensity data were taken from crystals mounted at the end of a glass fiber and held in place with epoxy adhesive. Crystal data and related parameters are given in Table 3. For 1′·2Me$_2$CO, 12 313 intensity data were collected, from which 11 735 unique observations remained after averaging of duplicate and equivalent measurements and deletion of systematic absences (R_{int} = 0.020), of these, 9709 with $I > 2\sigma(I)$; an absorption correction was applied based on 360 azimuthal scan data. For **6**·*n*-C$_5$H$_{12}$, of the 7725 intensity data (other than checks) collected, 7300 unique observations remained after averaging of duplicate and equivalent measurements and deletion of systematic absences (R_{int} = 0.029), of these, 5118 with $I > 2\sigma(I)$; an absorption correction was applied based on 720 azimuthal scan data. Both structures were solved by Patterson and Fourier methods. All non-hydrogen atoms were refined anisotropically. H atoms were added at calculated positions (C−H = 0.96 Å) with isotropic displacement parameters assigned as 1.2 times the equivalent isotropic U's of the corresponding C atoms. For the structure of **6**·2Me$_2$CO, a final difference electron density map showed seven peaks above 1 e Å^{-3} (max 1.82; largest diff hole −1.36 e Å^{-3}) lying closer than 1.1 Å from the Pt atoms. For the structure of **2**·*n*-C$_5$H$_{12}$, the atoms of the solvent molecule were refined isotropically and their C−C distances restrained to be near 1.54 Å. A final difference electron density map showed no peaks above 1 e Å^{-3} (max 0.92; largest diff hole −0.69 e Å^{-3}). For both structures, full-matrix least-squares refinement of the models against F^2 converged to final residual indices given in Table 3. All calculations were carried out using the SHELXL-93 program.[18]

Computational Details. A central difficulty in applying electronic structure methods to the polynuclear metal complexes under consideration is their big molecular size, involving 150−300 atoms, most of them being heavy atoms. To obtain

(18) Sheldrick, G. M. *SHELXL-93*, a program for crystal structure determination; University of Göttingen: Germany, 1993.

a computationally convenient size for the compounds, we used models resulting from substitution of the phenyl groups of the phosphido ligands by H atoms, while the C_6F_5 groups were replaced by the CF_3 ones. The use of such models does not alter the description of the "core" region of the compounds and is ultimately the most efficient and productive route to modeling the electronic structure and related properties of the polynuclear platinum complexes. The electronic and energetic properties of all model compounds were computed at the Becke's three-parameter hybrid functional[19] combined with the Lee−Yang−Parr correlation functional[20] abbreviated as B3LYP level of theory, using the LANL2DZ basis set[21] that includes Dunning/Huzinaga full DZ on first row and Los Alamos ECPs plus DZ for platinum and palladium atoms. The hybrid B3LYP functional was used, since it gives acceptable results for molecular energies and geometries, as well as proton donation, and weak and strong H-bonds.[3b,22] In all computations no constraints were imposed on the geometry. Full geometry optimization was performed for each structure using Schlegel's analytical gradient method,[23] and the attainment of the energy minimum was verified by calculating the vibrational frequencies that result in the absence of imaginary eigenvalues. All the stationary points have been identified for minimum (number of imaginary frequencies NIMAG = 0) or transition states (NIMAG = 1). All calculations were performed using the GAUSSIAN98 series of programs.[24] Moreover, the qualitative concepts and the graphs derived from the Chem3D program suite[25] highlight the basic interactions resulting from the DFT calculations.

Acknowledgment. We thank the Dirección General de Enseñanza Superior (Spain) for financial support (Project PB98-1595-C02-01). E.A. and A.M. acknowledge the Diputación General de Aragón or DGES (Spain) respectively for their grants.

Supporting Information Available: Tables of all atomic positional and equivalent isotropic displacement parameters, anisotropic displacement parameters, all bond distances and bond angles, hydrogen coordinates, and isotropic displacement parameters for the crystal structures of complexes **1′**·$2Me_2$-CO and **6**·*n*-C_5H_{12}. This material is available free of charge via the Internet at http://pubs.acs.org.

OM010407S

(19) Becke, A. D. *J. Chem. Phys.* **1992**, *96*, 2155. (b) Becke, A. D. *J. Chem. Phys.* **1993**, *98*, 5648.
(20) Lee, C.; Yang, W.; Parr, R. G. *Phys. Rev.* **1988**, *B37*, 785.
(21) Wadt, W. R.; Hay, P. J. *J. Chem. Phys.* **1985**, *82*, 5284.
(22) (a) Nicholas, J. B. *Top. Catal.* **1997**, *4*, 157. (b) Koch, W. R.; Hertwing, H. *Chem. Phys. Lett.* **1997**, *286*, 345. (c) Curtis, L. A.; Raghavachari, K.; Redfern, P. C.; Pople, J. A. *Chem. Phys. Lett.* **1997**, *270*, 419. (d) Smith, D. M.; Golding, B. T.; Radom, L. *J. Am. Chem. Soc.* **1999**, *121*, 9388. (e). Chandra, A. K.; Nguyen, M. T. *Chem. Phys.* **1998**, *232*, 299. (f) Nicholas, J. B. *Top. Catal.* **1999**, *9*, 181. (g) Arnaud, R.; Adamo, C.; Cossi, M.; Millet, A.; Vallé, Y.; Barone, V. *J. Am. Chem. Soc.* **2000**, *122*, 324.
(23) Schlegel, H. B. *J. Comput. Chem.* **1982**, *3*, 214.
(24) Frisch, M. J.; Trucks, G. W.; Schlegel, H. B.; Scusseria, G. E.; Robb, M. A.; Cheeseman, J. R.; Zakrzewski, V. G.; Montgomery, J. A.; Stratmann, R. E.; Burant, J. C.; Dapprich, S.; Millan, J. M.; Daniels, A. D.; Kudin, K. N.; Strain, M. C.; Farkas, O.; Tomasi, J.; Barone, V.; Cossi, M.; Cammi, R.; Mennucci, B.; Pomelli, C.; Adamo, C.; Clifford, S.; Orchterski, J.; Petersson, G. A.; Ayala, P. Y.; Cui, Q.; Morokuma, K.; Malick, D K.; Rabuck, A. D.; Raghavachari, K.; Foresman, J. B.; Cioslowski, J.; Ortiz, J. V.; Stefanov, B. B.; Liu, G.; Liashenko, A.; Piskorz, P.; Komaroni, I.; Gomperts, R.; Martin, R. L.; Fox, D. J.; Keith, T.; Al-Laham, M. A.; Peng, C. Y.; Nanayakkara, A.; Gonzalez, C.; Challacombe, M.; Gill, P. M.; Johnson, P.; Chen, W.; Wong, M. W.; Andres, J. L.; Head-Gordon, M.; Replogle, E. S.; Pople, J. A. *Gaussian 98*, revision A.4; Gaussian Inc.: Pittsburgh, PA, 1998.
(25) *ChemOffice 97*; Cambridge Scientific Computing, Inc.: 875 Massachusetts Ave., Suite 41, Cambridge, MA 02139.
(26) Alonso, E.; Forniés, J.; Fortuño, C.; Martín, A.; Orpen, A. G. *Organometallics* **2001**, *20*, 850.